

Rotary echo tests of coherence in Rydberg-atom excitation

Kelly Cooper Younge¹ and Georg Raithel

FOCUS Center, Department of Physics, University of Michigan, Ann Arbor, MI 48109, USA

E-mail: [kyoung@umich.edu](mailto:kyounge@umich.edu)

New Journal of Physics **11** (2009) 043006 (11pp)

Received 17 December 2008

Published 3 April 2009

Online at <http://www.njp.org/>

doi:10.1088/1367-2630/11/4/043006

Abstract. Rotary echoes are employed to study excitation dynamics in many-body Rydberg systems. In this method, a phase reversal of a narrow-band excitation field is applied at a variable time during the excitation pulse. The visibility of the resulting echo signal reveals the degree of coherence of the excitation process. Rotary echoes are measured for several $nD_{5/2}$ Rydberg levels of rubidium with principal quantum numbers near $n = 43$, where the strength of electrostatic Rydberg-atom interactions is modulated by a Förster resonance. The Rydberg-atom interactions are shown to diminish the echo visibility, in agreement with recent theoretical work. The equivalence of echo signals with spectroscopic data is demonstrated.

Contents

1. Introduction	2
2. Rotary echo sequences	2
3. Experimental setup for rotary echo tests	3
4. Results	4
5. Discussion and relation to other work	7
6. Conclusion	10
Acknowledgments	10
References	10

¹ Author to whom any correspondence should be addressed.

1. Introduction

The exaggerated properties of Rydberg atoms, such as large polarizabilities, long lifetimes and large size, lead to interactions that enable fundamental studies of quantum many-body systems [1, 2] and that are the basis for applications in quantum information processing [3, 4]. Of particular interest is the Rydberg excitation blockade, which follows from the spectral characteristics of the entangled many-body states that describe systems of interacting Rydberg atoms. Due to these interactions, the energy separation of the levels $|N, 0\rangle$ and $|N, 1\rangle$ differs from that of the levels $|N, k\rangle$ and $|N, k+1\rangle$, where k is the number of Rydberg excitations and N the number of atoms that coherently share these excitations. The level shifts prohibit narrow-band photo-excitation into levels $|N, k\rangle$ with $k > 1$. The blockade has been observed via reduced excitation rates [5]–[7] and narrowed excitation number distributions [8]. More recently, resonant energy transfer between cold atoms in spatially separated cylinders was observed [9], and the $|N, 0\rangle \rightarrow |N, 1\rangle$ and $|N, 1\rangle \rightarrow |N, 2\rangle$ transitions were spectroscopically measured [10].

One consequence of the coherent many-body nature of the states $|N, k\rangle$ is that the Rabi frequency between states $|N, 0\rangle$ and $|N, 1\rangle$ is given by $\Omega = \sqrt{N}\Omega_0$, where Ω_0 is the single-atom Rabi frequency [4]. The scaling of the Rabi frequency Ω with \sqrt{N} , which indicates collective, coherent dynamics, has been measured experimentally [11]. However, experimental work aimed at measuring the \sqrt{N} -enhancement of the Rabi frequency has been complicated by the fact that measurements in extended atom samples yield sums over many excitation domains, leading to rapid dephasing of the Rabi oscillations. Because of density gradients, the number of atoms per excitation domain, N , varies substantially over the excitation volume. Accounting for a weak dependence of the domain radius, r_b , on the local density, one finds a $\rho^{2/5}$ dependence of the Rabi frequency Ω on the local density, ρ , in the van der Waals regime [12] and a stronger $\rho^{2/3}$ dependence in the dipole–dipole regime. Rydberg atom Rabi oscillations have been measured previously as a demonstration of the coherence of Rydberg atom systems [13], but the observation of many oscillation cycles requires that the number of Rydberg excitations be limited to one or two [14].

2. Rotary echo sequences

Echo schemes, such as spin and rotary echo sequences, have been used extensively in the past to overcome the effects of inhomogeneities in many different systems [15, 16]. Recently, a rotary echo experiment was performed in a strongly interacting Rydberg gas to demonstrate coherence [17]. This experiment involves exciting atoms for a time τ_p , and then inverting the sign of the excitation amplitude. A many-body pseudoparticle approach, where groups of blockaded atoms are treated as ‘super-atoms’, is well suited to model this experiment in the strongly blockaded regime where $N \gg 1$ [12, 18]. In the pseudoparticle approach, the Hamiltonian describing the excitation is given by [19]

$$\hat{H}(t) = \sum_j \hat{H}_j(t) + \sum_{j < k} V_{jk} |n_j n_k\rangle \langle n_j n_k|,$$

$$\hat{H}_j(t) = -[\Delta\omega + \epsilon] |n_j\rangle \langle n_j| + \frac{\Omega_0}{2} \sqrt{N_j} (|g_j\rangle \langle n_j| + |n_j\rangle \langle g_j|), \quad (1)$$

where atomic units have been used. Here, the interaction V_{jk} is between pseudoparticles and not individual atoms. The kets $|g_j\rangle$ and $|n_j\rangle$ correspond to pseudoparticle j being in the ground state $|N_j, 0\rangle$ and excited state $|N_j, 1\rangle$, respectively, $\Delta\omega$ is the laser detuning (approximately zero in our case) and ϵ is a mean-field energy shift due to distant excited atoms. If $\Omega_0 \rightarrow -\Omega_0$ at $t = \tau_p$ and the terms ϵ and V_{jk} are negligible, the Hamiltonian in (1) exhibits near-perfect symmetry $\hat{H}(\tau_p - t) = -\hat{H}(\tau_p + t)$. Assuming that the excitation begins at $t = 0$, a rotary echo occurs at a time $2\tau_p$, when all pseudoparticles will be back in the ground state, regardless of their inhomogeneity in N_j . If ϵ and V_{jk} are significant and are not inverted, the Hamiltonian lacks this symmetry. The resultant decoherence of systems containing multiple pseudoparticles causes a reduction in echo visibility.

In the present paper, the rotary echo method is employed to study the effect of Rydberg-atom interactions on the coherence of excitation processes in many-body Rydberg-atom systems. The echo signal is recorded by varying τ_p for a fixed pulse length τ and counting the number of excitations. We show how the visibility of the rotary echo diminishes as the interaction strength, W , between Rydberg atoms is increased. We vary W by taking advantage of the interaction process $2 \times nD_{5/2} \rightarrow (n+2)P_{3/2} + (n-2)F_{7/2}$, which for Rb is nearly resonant at the principal quantum number $n = 43$. Due to this Förster resonance, W varies strongly as a function of n in the vicinity of $n = 43$, allowing us to realize cases from relatively weak interactions ($n = 40$) to strong interactions ($n = 43$) over a narrow range of n (see figure 3 of [20], where the behavior of the interactions in this range of n is explicitly shown). Rydberg excitation spectra, taken with and without excitation inversion, provide an alternate, equally valid test of coherence. In our work, we highlight the importance of atom-atom interactions in rotary echoes as well as the equivalence of such echoes with spectroscopic information.

3. Experimental setup for rotary echo tests

We cool and trap ^{85}Rb atoms in a magneto-optical trap and then form an optical dipole trap with a 5 W, 1064 nm laser beam focused through the center of the trap. The dipole trap has a temperature of approximately 1 mK and a peak density of 2.5×10^{11} atoms cm^{-3} . Atom samples are prepared at a repetition rate of 5 Hz and excited to $nD_{5/2}$ Rydberg states using the two-photon excitation $5S_{1/2} \rightarrow 5P_{3/2} \rightarrow nD_{5/2}$ (see figure 1(a)). The excitation is performed with two narrow-linewidth, coincident laser pulses propagating in orthogonal directions, as shown in figure 1(b). The pulses have a square temporal profile with a width of 120 ns. The lower transition laser beam is focused to a full-width at half-maximum (FWHM) of the intensity of $18 \mu\text{m}$ and has a peak Rabi frequency of $\Omega_1 = 2\pi \times 10$ MHz. The laser is detuned from the intermediate $5P_{3/2}$ state by $\delta = 2\pi \times 130$ MHz. The upper transition laser beam is focused to a FWHM of $8 \mu\text{m}$, and has a peak Rabi frequency of $\Omega_2 \approx 2\pi \times 10$ MHz. These conditions result in a Rabi frequency at the two-photon resonance of $\frac{\Omega_1\Omega_2}{2\delta} \approx 2\pi \times 400$ kHz, with less than 0.01 spontaneous emission events per atom on the lower transition. Both lasers have a linewidth $\delta\nu/2\pi \lesssim 2$ MHz. For typical experimental conditions there are about 500 ground-state atoms in the excitation volume. The number of atoms per blockaded region, N , reaches a maximum of about 100 at $n = 43$. We apply a state-selective field ionization (SSFI) ramp 100 ns after excitation to ionize the Rydberg atoms, and detect the freed electrons with a microchannel plate (MCP) detector. To perform the rotary echo experiment, we shift the phase of the radio

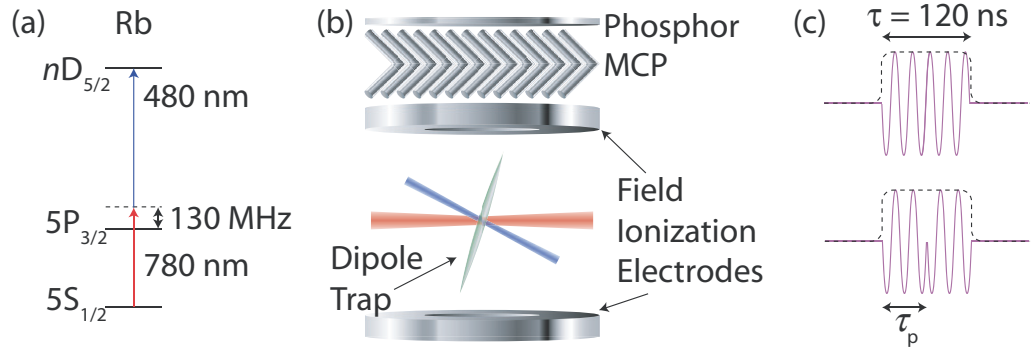


Figure 1. Experimental setup. (a) Rydberg atom excitation scheme. (b) Excitation geometry and detection scheme with microchannel plate (MCP). (c) RF signal sent to the AOM used to control the upper transition laser pulse for the case without phase inversion (top) and with phase inversion at time τ_p (bottom).

frequency (RF) applied to the acousto-optic modulator (AOM) that controls the upper-transition light pulse by π after a time τ_p , as illustrated in figure 1(c). This accomplishes the inversion of Ω_0 in (1).

4. Results

Figure 2(a) shows the rotary echo signal for the Rydberg state $40D_{5/2}$. For each data point, the atoms are excited for a time τ_p and then the evolution is reversed for a time $\tau - \tau_p$ (pulse width $\tau = 120$ ns). Each point represents 200 averages. Similar to a convention used in [17], for the visibility of the echo we use

$$\frac{N_R(\tau_p = 0) + N_R(\tau_p = \tau) - 2 N_R(\tau_p = \tau/2)}{N_R(\tau_p = 0) + N_R(\tau_p = \tau) + 2 N_R(\tau_p = \tau/2)}. \quad (2)$$

The visibility obtained for $40D_{5/2}$ is 0.67 ± 0.11 , which is on the high side of what was achieved in [17]. Standard error propagation techniques are used to arrive at the quoted uncertainty. The slight asymmetry of the curve is most likely due to small asymmetries in the short pulse used for excitation. For example, the pulse may have slightly more amplitude in the beginning than at the end, which would explain why the echo signal of figure 2 is shifted by a small amount earlier in time. We believe that the visibility does not reach 100% because of residual interactions and the laser linewidths (~ 2 MHz), which affect the magnitudes of the terms V_{jk} and $\Delta\omega$ in (1), respectively. Also, the measured curves in figure 2(b) appear to be slightly wider than the corresponding curves in figure 2(c); we attribute this to the laser linewidths as well.

According to the principle that time-domain and spectroscopic information are generally equivalent, evidence for the coherence of the evolution cannot only be obtained via rotary echoes but also by spectroscopy of the excited Rydberg level. We record the number of Rydberg excitations as a function of the 480 nm excitation laser frequency, ν_b , with and without the phase inversion of the RF applied to the AOM. Figure 2(b) shows spectra obtained by scanning ν_b across the two-photon resonance. The fact that the spectrum with phase inversion (circles) in figure 2(b) closely resembles the dashed line in figure 2(c) supports our interpretation

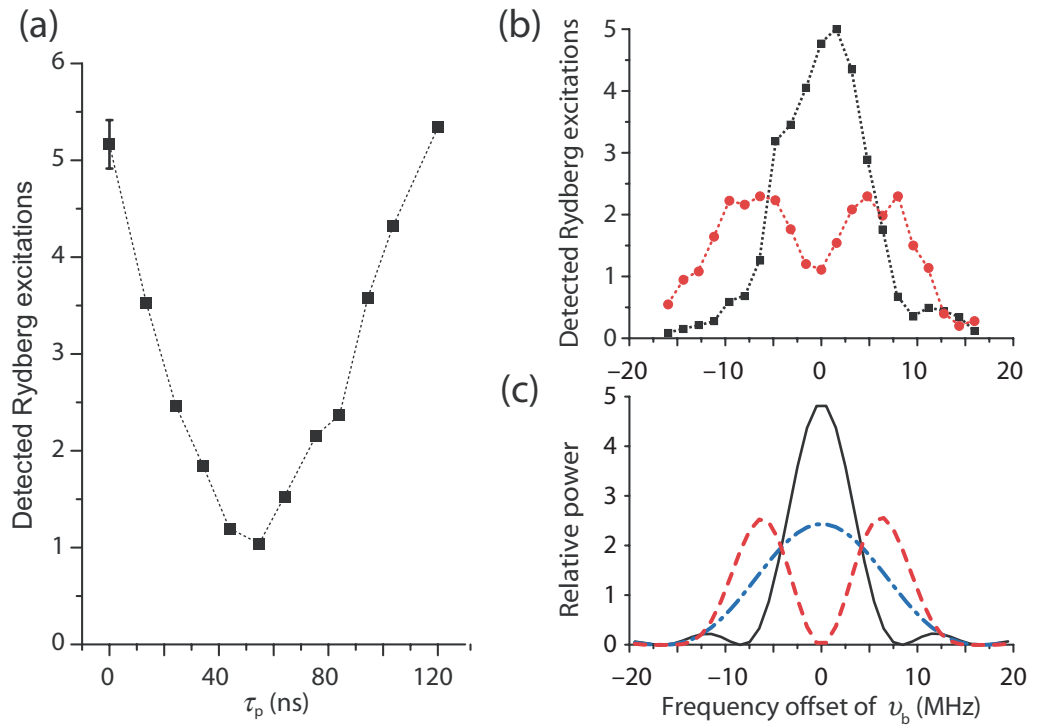


Figure 2. Echo data and spectra for the state $40D_{5/2}$ for square excitation pulses. (a) Number of Rydberg atoms for pulses with duration $\tau = 120$ ns, detected as a function of τ_p , the time of the phase flip with respect to the beginning of the excitation pulse. (b) Excitation spectra without phase inversion (black squares) and with phase inversion at $\tau_p = 60$ ns (red circles). (c) Power spectra of three different square pulses. Black line: $\tau = 120$ ns and constant phase. Red dashed line: $\tau = 120$ ns and phase flip at $\tau_p = \tau/2$. Blue dash-dotted line: $\tau = 60$ ns square pulse without phase flip and with twice the intensity of the other two pulse types.

of coherent excitation. In both the measured spectrum and the corresponding calculated power spectrum (dashed curve), the separation between the two resolved peaks is ~ 13 MHz. If the Rydberg excitation was not coherent, the excitation pulse with phase inversion at $\tau_p = \tau/2 = 60$ ns would act as two independent 60 ns pulses. These would generate an excitation spectrum with twice the width and half the amplitude of the spectrum obtained with the 120 ns pulse absent the phase inversion (dash-dotted line in figure 2(c)).

Noting that the pulse used in figure 2(b) represents a coherent sequence of two half-pulses (of opposite phase), it is not surprising that the spectrum in figure 2(b) resembles spectra obtained with Ramsey's well-known separated oscillatory field method. In both cases, the presence of spectral modulations signifies coherent evolution. Differences between typical conditions used in the separated-field method and the present work include the time separation between the pulses (vanishing in our case), and the significance of excitation saturation and the detuning during excitation (both high in our case).

To measure the effect of Rydberg–Rydberg interactions on the echo visibility, we enhance the interaction strength, W , by varying the n value of the excited Rydberg state. We verify experimentally the relative interaction strengths of different Rydberg states by recording the

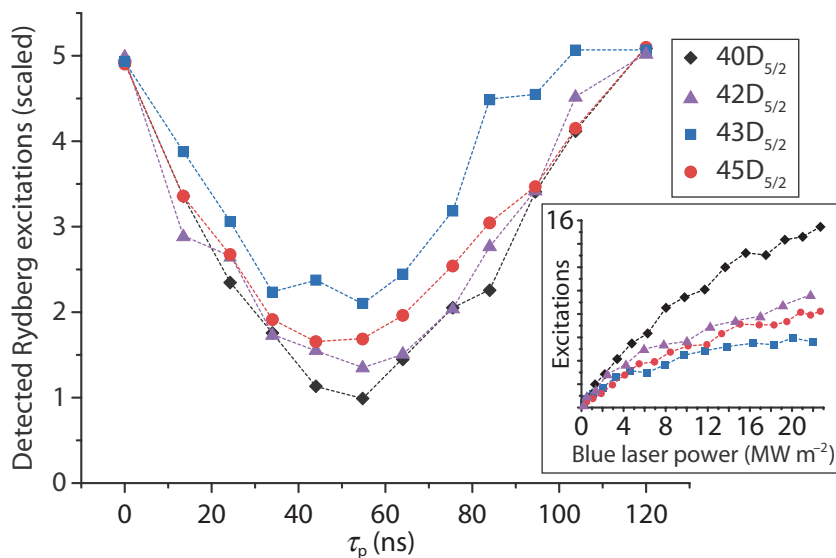


Figure 3. Number of Rydberg atoms detected as a function of τ_p for the states $40D_{5/2}$ (black diamonds), $42D_{5/2}$ (green triangles), $43D_{5/2}$ (red circles) and $45D_{5/2}$ (blue squares). For ease of comparison, all curves are scaled to a value of five at $\tau_p = 0$ and 120 ns. The inset shows the number of Rydberg atoms detected as a function of upper transition laser power for the same set of states. The degree of saturation reflects the strength of atom–atom interactions.

number of Rydberg excitations as a function of the upper transition laser power for different n . As a consequence of the Rydberg excitation blockade, the interactions between atoms lead to saturation in the number of excitations as the laser power is increased [5]. The saturation is more prominent for more strongly interacting Rydberg states. The inset of figure 3 shows the number of detected Rydberg excitations as a function of upper transition laser power for several Rb $nD_{5/2}$ states. The excitation number for $40D_{5/2}$, the state with the weakest interactions studied in this paper, shows the least amount of saturation. Conversely, the excitation number saturates much more significantly for $43D_{5/2}$, the state exhibiting the strongest interactions (because it is closest to the center of the Förster resonance). For the states $42D_{5/2}$ and $45D_{5/2}$ we observe intermediate saturation behavior, according to their moderate interaction strengths (see figure 3(a) of [20]). The saturation curve of figure 3 provides additional insight into the special case of $n = 40$, where the interaction due to the Förster resonance that is centered at $n = 43$ is nearly equal and opposite in sign to the sum of the effect of all other interaction channels. From the saturation curve, one can see that while the interactions at $n = 40$ are clearly less than those for $n = 42, 43$ and 45 , there is still residual interaction leading to saturation in the excitation number. It is primarily for this reason that perfect echo visibility is not achieved for this case, in addition to the laser linewidths. For states below $n = 40$, the cancellation of the interactions is less perfect, and thus the visibilities would initially decrease for n immediately below 40. If even lower n were used, the visibilities would be expected to eventually improve, as the van der Waals shifts scale as n^{11} .

We record the echo signal for $n = 42, 43$ and 45 using the same experimental procedure as described above. The upper transition laser power used is scaled proportional to n^{*3} , with effective quantum number n^* , to give the same single-atom Rabi frequency for each state; for $n = 43$ the intensity is 5.8 MW m^{-2} . The results are shown in figure 3. The curves

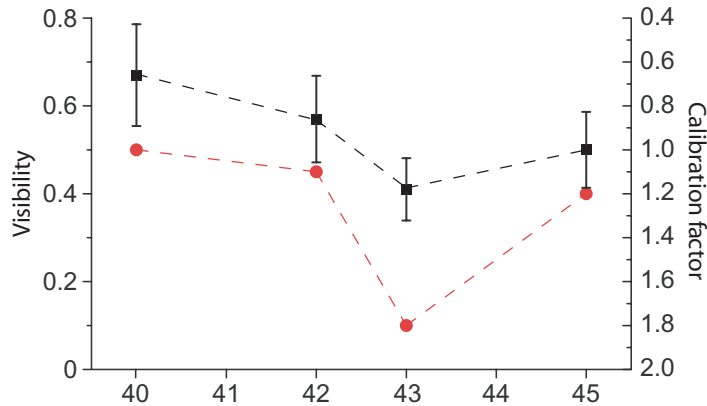


Figure 4. Echo visibilities (squares, left axis) and calibration factors (circles, right axis) for each n state examined.

are multiplied by scaling factors such that the average values of the counts for $\tau_p = 0$ and 120 ns are five for each curve. The scaling factors reflect the varying degree of interactions; stronger interactions lead to more saturation and thus larger scaling factors (see figure 4). From (2), the echo visibilities for $n = 40, 42, 43$ and 45 , obtained from the data shown in figure 3, are 0.67 ± 0.11 , 0.57 ± 0.10 , 0.41 ± 0.07 and 0.50 ± 0.09 , respectively. The trends of echo visibility and saturation behavior as a function of n are compared in figure 4. The figure clearly demonstrates that saturation behavior and loss in echo visibility are closely correlated.

Finally, we have recorded the excitation spectra analogous to the spectrum shown in figure 2(b) for $n = 42, 43$ and 45 . The results are shown in figure 5. The visibility of the two side peaks for the case where the excitation amplitude is inverted (red circles) decreases as the atom–atom interaction strength increases. The echo data and spectroscopic data presented in this paper allow us to conclude that increased atomic interactions and the resultant decoherence in pseudoparticle evolution have complementary consequences in the dynamics and the spectral properties of many-body Rydberg systems, namely a loss of visibility in rotary echo curves (figure 3) and a loss of contrast in spectral data (figures 2(b) and 5).

5. Discussion and relation to other work

We first discuss our results in context with recent theoretical calculations performed by Hernandez and Robicheaux [19]. We first note that the system studied in our paper is characterized by many-body interactions between pseudoparticles (as opposed to interactions between individual atoms); this statement follows from the saturation behavior shown in figure 3 and from estimates of N_j based on the measured ground-state and Rydberg atom numbers. In [19], echo visibilities are calculated for three cases: a sparse system where the interaction V_{jk} is negligible, a perfectly blockaded system in which only one Rydberg excitation is allowed in the entire excitation volume, and an intermediate system in between these two limiting cases. A perfect echo visibility is achieved for the first two cases, whereas the echo is reduced for the third case when V_{jk} is no longer negligible. We believe that our results for the state $40D_{5/2}$ approach the limiting case in which the interaction between particles is at a minimum and,

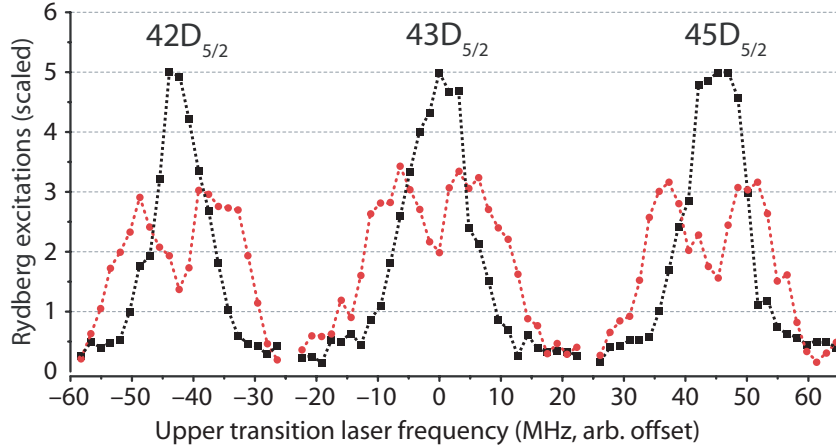


Figure 5. Excitation spectra for the states $42D_{5/2}$, $43D_{5/2}$ and $45D_{5/2}$. The black squares show the case where the excitation amplitude is constant throughout the pulse, and the red circles show the results when $\tau_p = \tau/2$. The number of detected excitations is scaled to give a maximum excitation number of five.

hence, the best echo visibility is achieved. The results for the states $42D_{5/2}$, $43D_{5/2}$ and $45D_{5/2}$ correspond to the intermediate case in [19], where the role of atomic interactions is sufficiently strong to cause a reduction in echo visibility, but not strong enough to turn the entire excitation volume into a single excitation domain. In this regime, the interactions cause both a loss in echo visibility and a reduction in the number of excitations due to the blockade effect. In the present experiment, the regime of a single excitation was not realized. One way to achieve a single excitation domain would be to excite the strongly interacting state $43D_{5/2}$ in a smaller excitation volume. For our current experimental parameters, we excite approximately three $43D_{5/2}$ Rydberg atoms per experiment. Thus, the excitation volume would need to be reduced by a factor of at least three before the limiting case of a single excitation domain would be achieved.

To interpret the loss of visibility in the intermediate regime observed as the interaction strength increases, we compare the terms $\sqrt{N_j}\Omega_0$ and V_{jk} in (1), expanding on arguments presented in [12]. Assuming a power law, $W \propto C_p d^{-p}$, for the Rydberg-atom interaction W as a function of interatomic separation d , and assuming that the laser linewidth $\delta\nu_L$ satisfies $\sqrt{N_j}\Omega_0 \gg \delta\nu_L$, the excitation domain radius, r_b , is found to scale as $C_p^{2/(2p+3)} \rho^{-1/(2p+3)}$. Here, $\delta\nu_L$ is the laser linewidth, ρ is the ground-state atom density, and $p = 3$ for resonant electric-dipole interactions and $p = 6$ for van der Waals interactions. Further, $V_{jk} = \langle C_p d_{lm}^{-p} \rangle$, where the indices l and m identify a random atom pair with atom l in domain j and atom m in domain k , and $\langle \dots \rangle$ identifies an average with weighting factor given by the probability of finding a pair of Rydberg excitations on atoms l and m . Assuming an efficient blockade, consistent with the experimentally observed saturation, one may expect $\langle d_{lm}^{-p} \rangle \approx [2r_b]^{-p}$. It follows that $\sqrt{N_j}\Omega_0$ and V_{jk} are identical and scale as $\rho^{p/(2p+3)} C_p^{3/(2p+3)}$. Consequently, the time-dependent Schrödinger equation that follows from (1) becomes invariant under variations of density, ρ , and interaction strength, C_p , if an excitation pulse is used that is invariant as a function of a scaled time, $\tilde{t} \propto t \rho^{p/(2p+3)} C_p^{3/(2p+3)}$ (t is the physical time). Since in our experiment we keep the timing of the physical pulse fixed, stronger interactions correspond to longer scaled

times \tilde{t} . Since longer scaled times lead to more strongly excited domains, we conclude that the reduced visibilities, observed for stronger interactions in the intermediate regime, are a result of driving the domains further into their first excited states, $|N_j, 1\rangle$. Interestingly, in this model the reduced visibilities *do not* result from an enhancement of the V_{jk} terms relative to the $\sqrt{N_j}\Omega_0$ terms in (1). It is noted that longer scaled times can also be achieved by simply increasing the physical pulse duration while keeping all other conditions the same. We did, indeed, observe a trend that longer physical pulse durations lead to less visible echoes. Finally, we note that the longer scaled times, realized in the cases of stronger interactions in figure 3, may also be the reason why the signal minima appear to be shifted slightly toward earlier times as the interaction strength increases.

A critical assumption made in the above is that $\langle d_{lm}^{-p} \rangle \approx [2r_b]^{-p}$. In a perfectly blockaded atom sample, the validity of this assumption is ensured by a drastic suppression of the pair correlation function of Rydberg excitations for Rydberg–Rydberg separations $d < 2r_b$ [21]. Systems with a reduced blockade effectiveness will exhibit a less dramatic suppression of the pair correlation function at small distances. A reduction in blockade effectiveness can result from several reasons, including the excitation bandwidth, anisotropy and ‘dead angles’ in the Rydberg–Rydberg interaction, and motion-induced decoherence during excitation. A loss of structure in the Rydberg pair correlation will obviously lead to a more random spread of Rydberg excitations over all atoms in the sample. Consequently, the condition $\langle d_{lm}^{-p} \rangle \approx [2r_b]^{-p}$ will trend toward $\langle d_{lm}^{-p} \rangle \gg [2r_b]^{-p}$ (for large and positive p). We have verified this trend in simulations. The trend simply arises from the likelihood of finding Rydberg-atom pairs at small separations d_{lm} . A few instances of small separations are sufficient to strongly inflate the expectation value for $\langle d_{lm}^{-p} \rangle$, because d_{lm}^{-p} quickly diverges at small d_{lm} (for large and positive p). Thus, the assumption $\langle d_{lm}^{-p} \rangle \approx [2r_b]^{-p}$, the effectiveness of the Rydberg excitation blockade, and the validity of the model underlying (1) are intimately related to each other.

In the following, we compare our results with a recent experiment described in [17]. For the case of least interaction ($n = 40$), we find a maximum echo visibility of 0.67, which is about 0.10 higher than the largest echo visibility obtained in [17], recorded in their case of lowest density. In [17], a trap temperature as low as $3.8 \mu\text{K}$ was used, which allowed for longer coherence times than would be obtainable in our 1 mK trap. The highest trap density used in [17] was $\sim 5 \times 10^{13} \text{ atoms cm}^{-3}$ and typical excitation pulse lengths were $\sim 500 \text{ ns}$. We have shown in the present experiment that an excellent echo visibility is achievable in a much hotter sample by performing the experiment with shorter pulses and using densities that are about two orders of magnitude lower than those used in [17]. A substantial difference between the work in [17] and our work is that our work has been performed with D-Rydberg levels, whereas the data in [17] have been obtained with the 43S level. The fact that we observe substantial rotary echoes despite that difference is noteworthy for two reasons. Firstly, $D_{5/2}$ -levels in Rb have stronger, attractive and anisotropic interactions, whereas S-levels have weaker, repulsive and isotropic interactions (see figures 3 and 6 of [20], respectively). The $nD_{5/2}$ -states in Rb shift because of couplings to states with angular momenta that allow for so-called ‘Förster zeroes’ (i.e., binary molecular Rydberg states with little interaction [22]), whereas S-states do not have Förster zeroes. Our results show that these differences do not preclude considerable echo visibility in systems of interacting Rb $nD_{5/2}$ Rydberg atoms. Secondly, the $nD_{5/2}$ -levels of Rb exhibit a Förster resonance at $n = 43$ while S-levels exhibit a more generic van der Waals-type interaction. The Förster resonance leads to substantial populations of Rydberg levels in

the Förster-resonant states, as demonstrated earlier [23]. The results for $43D_{5/2}$ presented in the present paper show that the Förster-resonance-induced state mixing does not cause a breakdown of echo visibility.

6. Conclusion

We have demonstrated coherent excitation of Rb $nD_{5/2}$ Rydberg atoms using a rotary echo method. Echo signals and excitation spectra are found equally valid in providing evidence of such coherence. We have varied the strength of the atom–atom interactions by performing the experiment with Rydberg states near a Förster resonance where the interaction features an abrupt change in magnitude and a zero-crossing at $n = 40$. We have shown that the echo visibility is reduced as the strength of the interaction increases. We have interpreted this behavior by examining the Hamiltonian of the system given in (1). To improve the echo visibility in the case of strongly interacting Rydberg-atom systems, in future work one may look for ways to invert all terms in the Hamiltonian given in (1) (as opposed to just the terms $\sqrt{N_j}\Omega_0$). This could be accomplished by exploiting the abrupt change in sign of atomic interactions in the vicinity of Förster resonances [19].

Acknowledgments

We acknowledge helpful conversations with P Berman and F Robicheaux. KCY acknowledges support from the NDSEG fellowship. This work was supported by NSF grant nos PHY-0555520 and PHY-0114336.

References

- [1] Côté R 2000 *Phys. Rev. Lett.* **85** 5316–9
- [2] Mudrich M, Zahzam N, Vogt T, Comparat D and Pillet P 2005 *Phys. Rev. Lett.* **95** 233002
- [3] Jaksch D, Cirac J I, Zoller P, Rolston S L, Côté R and Lukin M D 2000 *Phys. Rev. Lett.* **85** 2208–11
- [4] Lukin M D, Fleischhauer M, Côté R, Duan L M, Jaksch D, Cirac J I and Zoller P 2001 *Phys. Rev. Lett.* **87** 037901
- [5] Tong D, Farooqi S M, Stanojevic J, Krishnan S, Zhang Y P, Côté R, Eyler E E and Gould P L 2004 *Phys. Rev. Lett.* **93** 063001
- [6] Vogt T, Viteau M, Zhao J, Chotia A, Comparat D and Pillet P 2006 *Phys. Rev. Lett.* **97** 083003
- [7] Vogt T, Viteau M, Chotia A, Zhao J, Comparat D and Pillet P 2007 *Phys. Rev. Lett.* **99** 073002
- [8] Cubel Liebisch T, Reinhard A, Berman P R and Raithel G 2005 *Phys. Rev. Lett.* **95** 253002
- [9] van Ditzhuijzen C S E, Koenderink A F, Hernandez J V, Robicheaux F, Noordam L D and van den Heuvel H B 2008 *Phys. Rev. Lett.* **100** 243201
- [10] Reinhard A, Younge K C, Liebisch T C, Knuffman B, Berman P R and Raithel G 2008 *Phys. Rev. Lett.* **100** 233201
- [11] Heidemann R, Raitzsch U, Bendkowsky V, Butscher B, Löw R, Santos L and Pfau T 2007 *Phys. Rev. Lett.* **99** 163601
- [12] Hernandez J V and Robicheaux F 2008 *J. Phys. B: At. Mol. Opt. Phys.* **41** 045301
- [13] Reetz-Lamour M, Amthor T, Deiglmayr J and Weidemüller M 2008 *Phys. Rev. Lett.* **100** 253001
- [14] Johnson T A, Urban E, Henage T, Isenhower L, Yavuz D D, Walker T G and Saffman M 2008 *Phys. Rev. Lett.* **100** 113003
- [15] Hahn E L 1950 *Phys. Rev.* **80** 580

- [16] Solomon I 1959 *Phys. Rev. Lett.* **2** 301
- [17] Raitzsch U, Bendkowsky V, Heidemann R, Butscher B, Löw R and Pfau T 2008 *Phys. Rev. Lett.* **100** 013002
- [18] Robicheaux F 2005 *J. Phys. B: At. Mol. Opt. Phys.* **38** S333
- [19] Hernandez J V and Robicheaux F 2008 *J. Phys. B: At. Mol. Opt. Phys.* **41** 195301
- [20] Reinhard A, Liebisch T C, Knuffman B and Raithel G 2007 *Phys. Rev. A* **75** 032712
- [21] Robicheaux F and Hernandez J V 2005 *Phys. Rev. A* **72** 063403
- [22] Walker T G and Saffman M 2005 *J. Phys. B: At. Mol. Opt. Phys.* **38** S309–19
- [23] Reinhard A, Liebisch T C, Younge K C, Berman P R and Raithel G 2008 *Phys. Rev. Lett.* **100** 123007